Electrochemistry Communications 76 (2017) 10–14

Contents lists available at ScienceDirect

Electrochemistry Communications

journal homepage: www.elsevier.com/locate/elecom

Fabrication of irregular-layer-free and diameter-tunable Ni–Ti–O nanopores by anodization of NiTi alloy

Ruiqiang Hang [a,*], Ya Zhao [a], Long Bai [a], Yanlian Liu [a], Ang Gao [b], Xiangyu Zhang [a], Xiaobo Huang [a], Bin Tang [a], Paul K. Chu [b]

[a] Research Institute of Surface Engineering, Taiyuan University of Technology, Taiyuan 030024, China
[b] Department of Physics and Materials Science, City University of Hong Kong, Tat Chee Avenue, Kowloon, Hong Kong, China

ARTICLE INFO

Article history:
Received 30 November 2016
Received in revised form 11 January 2017
Accepted 11 January 2017
Available online 13 January 2017

Keywords:
Nickel–titanium alloy
Anodization
Nanopores

ABSTRACT

Ni–Ti–O nanopores (NPs) free of irregular surface layers and with tunable diameters are prepared by anodizing NiTi alloy in glycerol containing H_2O and NaCl. In an electrolyte composed of glycerol, 10 vol% H_2O and 0.6 M NaCl, NPs with diameters between 23 and 39 nm can be produced at anodization voltages between 20 and 80 V. In this electrolyte system, the irregular oxide layer on the surface can be completely removed chemically and/or mechanically during anodization. The resulting Ni–Ti–O NPs with tunable diameters should prove useful, for example, in energy, environmental and biomedical applications.

1. Introduction

Anodization of nearly equiatomic NiTi alloy to generate Ni–Ti–O nanotubes (NTs) was first reported by Kim and co-workers, who used ethylene glycol (EG) containing H_2O and NH_4F as the electrolyte [1]. They found that the NTs possessed a high rate capability and excellent cycling stability, suggesting that they would perform well as electrode materials in pseudocapacitors. Subsequent investigations showed that the NTs were also promising in gas sensing [2,3], biosensing [4], electrocatalysis [5,6], and biomedical engineering [7–11]. In many of these applications, a large specific surface area is crucial to achieving high efficiency [12]. However, Ni–Ti–O NTs possess a relatively small specific surface area due to their limited length (<1.3 μm) [13], which may be ascribed to aggressiveness of the F^- ions to the NTs during anodization. Our previous work revealed that Cl^- could substitute for F^- [14] and in an electrolyte composed of EG, H_2O and HCl, Ni–Ti–O nanopores (NPs) as long as 160 μm were synthesized. Nonetheless, the NPs prepared in the EG-based electrolyte have two shortcomings, namely the irregular surface layer, which is difficult to remove, and the fact that the diameter of the NPs cannot easily be tailored [14], which limits wider application of the materials. For example, the irregular layer may hinder electron and ion transport in charging–discharging, thus compromising the material's pseudocapacitive properties [1], and some diameter-dependent properties have also been observed [12]. It is therefore highly desirable to fabricate irregular-layer-free and diameter-tunable Ni–Ti–O NPs. In the work reported here, a new electrolyte composed of glycerol, H_2O and NaCl is employed to fabricate the Ni–Ti–O NPs and it is shown that, under specific conditions, diameter-tunable NPs without an irregular surface layer can be anodically produced on the NiTi alloy.

2. Materials and methods

A NiTi alloy (50.8 at.% Ni) rod (Φ9 mm produced by Xi'an SaiTe Metal Materials Development Co., Ltd., China) was cut into disks 2 mm thick, polished, ultrasonically cleaned, and dried in cool air. Anodization of the NiTi samples was carried out in 100 ml of the electrolyte comprising glycerol, H_2O and NaCl using a power supply (IT6123, ITECH, China) at room temperature (~30 °C). The anodization time was 10 min unless otherwise specified. The electrolyte composition and anodization voltage were varied to investigate their respective influence on anodic growth of the NPs. Nano Measure 1.2 software (Fudan University, China) was used to measure the pore size. 30 pores were measured for each group and their average value and standard deviation are shown. The steady-state electrolyte temperature near the sample was measured using a thermometer. A field-emission scanning electron microscope (FE-SEM, JSM-7001F, JEOL) equipped with an energy-dispersive X-ray spectroscope (EDS, QX200, Bruker) was utilized to observe the morphology and detect the elemental composition of the anodized samples.

* Corresponding author.
E-mail address: hangruiqiang@tyut.edu.cn (R. Hang).

http://dx.doi.org/10.1016/j.elecom.2017.01.010
1388-2481/

3. Results

Fig. 1(a) presents the surface SEM images of the samples anodized at 20 V in glycerol containing different amounts of H_2O and NaCl. The low- and medium-magnification images show that increasing the H_2O and NaCl content leads to increased surface roughness. The high-magnification images reveal no well-defined structures when the sample is anodized in an electrolyte containing 5 vol% H_2O and 0.3 M NaCl. In contrast, NPs can be clearly observed when the sample is anodized in an electrolyte containing 10 vol% H_2O and 0.6 M NaCl, but further increasing the content of H_2O and NaCl generates nanoporous structures that are not well defined. The corresponding current density–time curves in Fig. 1(b) show that the initial current densities drop quickly and that large amounts of H_2O and NaCl in the electrolyte elevate the steady-state current densities.

Fig. 2(a) and (b) show the low- and high-magnification surface SEM images, respectively, of samples anodized at 20–90 V in glycerol containing 10 vol% H_2O and 0.6 M NaCl. When the voltage is between 20 and 40 V, a uniform surface morphology can be seen. In contrast, a high voltage (50–90 V) leads to uneven and flaky exfoliation and more severe spalling can be seen at higher voltages. The high-magnification SEM images show that when the voltage is between 20 and 50 V, the pore diameter decreases gradually but that increasing the voltage above 50 V unexpectedly leads to a slight increase in the pore diameter. When the voltage is 90 V, a well-defined nanoporous structure cannot be produced. Generally, the NP length increases with anodization voltage and high-magnification images of the samples anodized at 30 and 50 V examples are shown in the insets. The electrolyte also changes, as shown in Fig. 2(c). When the voltage is low (20–40 V), smoke-like substances are observed in the beakers, whereas many small pieces appear to come off from the samples into the electrolyte when the voltage is high (50–90 V). The current density–time curves in Fig. 2(d) also exhibit two distinct tendencies. A low voltage (20–40 V) leads to a steady-state current density, but high voltage (60–90 V) results in gradually increasing current densities with narrow periodic fluctuations after an initial quick drop. Although the curve recorded at 50 V shows periodic fluctuations, the cycle is relatively long and there is no sign of gradual increase in the current density. Fig. 2(e) presents the variation in the pore diameter as a function of anodization voltage. The diameter decreases from 39 nm at 20 V to 23 nm at 50 V and further increasing the voltage only increases the pore diameter slightly. The electrolyte temperature as a function of voltage is displayed in Fig. 2(f) and three different regions may be defined. In the range between 20 and 40 V, the temperature is very close to room temperature (30 °C). When the voltage is between 50 and 80 V, the temperature increases slowly from 33 °C at 50 V to 37 °C at 80 V, while a high voltage of 90 V rapidly raises the temperature to 50 °C.

Fig. 3 shows the surface SEM images of samples anodized at 40 V and 70 V for different periods of time. When a sample is anodized at 40 V (Fig. 3(a)), the anodization time has little influence, as shown by the low-magnification morphologies. The high-magnification images show that after anodization for 1 min, the thin irregular surface layer

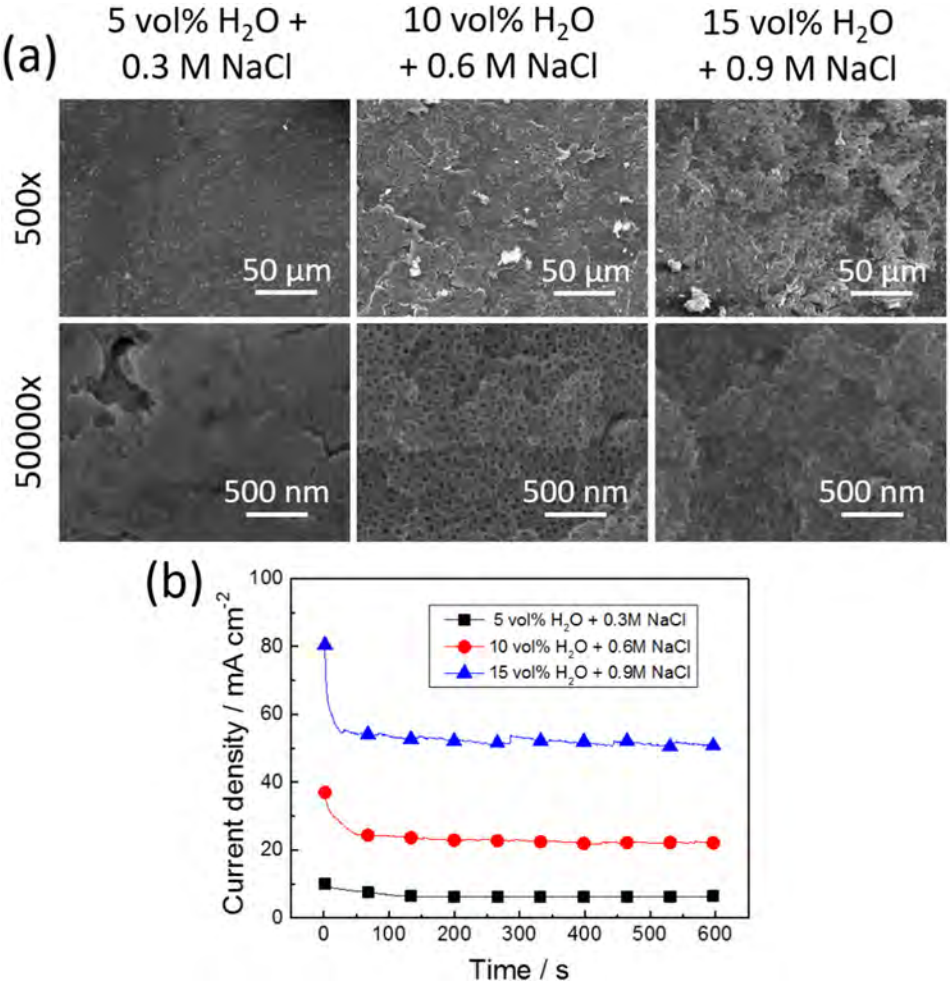

Fig. 1. (a) Surface SEM images of the samples anodized at 20 V in glycerol containing different H_2O and NaCl contents; (b) current density–time curves acquired from the samples.

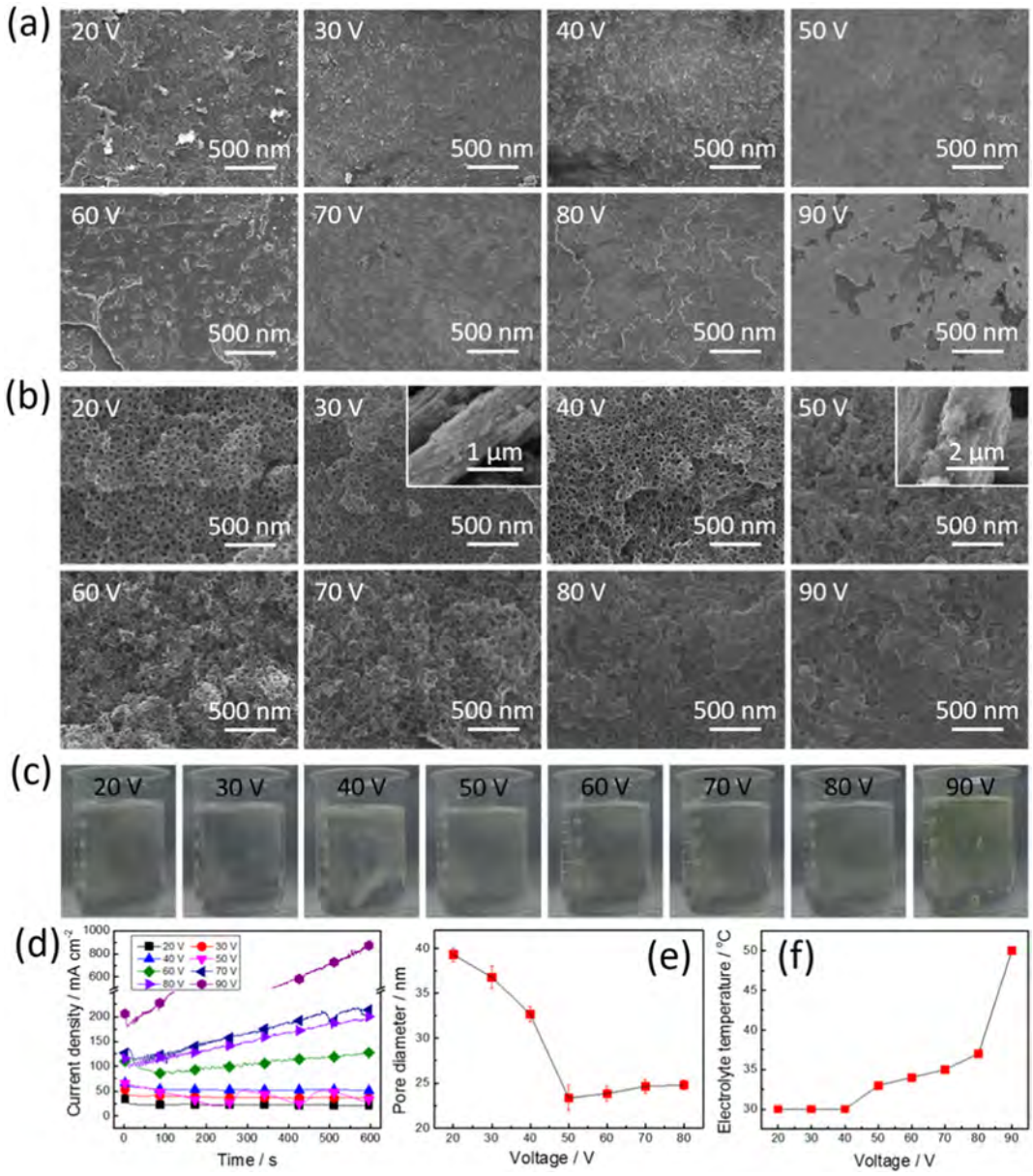

Fig. 2. (a) Low-magnification and (b) high-magnification surface SEM images of the samples anodized at 20–90 V in glycerol containing 10 vol% H_2O and 0.6 M NaCl. The anodization voltage of each sample is shown on upper right corner of each image. Insets in high-magnification images of the samples anodized at 30 and 50 V show their respective cross-sectional morphology. (c) Optical images of the electrolytes in the electrolytic cells after anodization of the samples at 20–90 V. (d) Current density–time curves of the samples; (e) NP diameter as a function of anodization voltage; (f) electrolyte temperature as a function of anodization voltage.

is partially removed, and after anodization for 2 min, it is removed completely, exposing ordered NPs. When the voltage is raised to 70 V (Fig. 3(b)), the low-magnification images show uneven flaky exfoliation. A longer anodization time generally leads to a larger spalling area. The high-magnification images show that most of the surface is covered by an irregular layer in the initial stage of anodization and that ordered NPs are only exposed in the peeled area. However, after anodization for 10 min, the irregular surface layer is completely removed, thereby exposing all the underlying NPs.

4. Discussion

Although Ni–Ti–O NPs can be fabricated in an electrolyte composed of EG, H_2O and HCl [14], the adherent irregular surface layer and constant pore diameter present obstacles to wider application [15,16]. In this work, these two drawbacks can be overcome by using a different electrolyte consisting of glycerol, H_2O and NaCl. The anodization voltage affects the NT and NP diameters [17,18] but in the EG-based electrolyte, the optimal voltage to prepare Ni–Ti–O NPs on NiTi is restricted to about 10 V and so the pore diameter is essentially fixed [14]. However, using a glycerol-based electrolyte widens the voltage window (20–80 V), making it possible to produce NPs with different diameters. This may be ascribed to the different viscosities of EG and glycerol. The viscosity of glycerol is about 68 times that of EG at the same temperature [19] and a large viscosity may convert the rate-limiting step in anodization from the electrochemical reaction at the electrode/electrolyte interface to diffusion of reactants to the interface [20]. Since the electrochemical reaction is sensitive to the applied voltage but diffusion is less sensitive, a viscous electrolyte may reduce the sensitivity of the overall anodization process to the applied voltage, resulting in a larger voltage window. In general, the diameter of the TiO_2 NTs prepared on pure Ti by anodization is positively related to the voltage [21]. However, Ni–Ti–O NPs

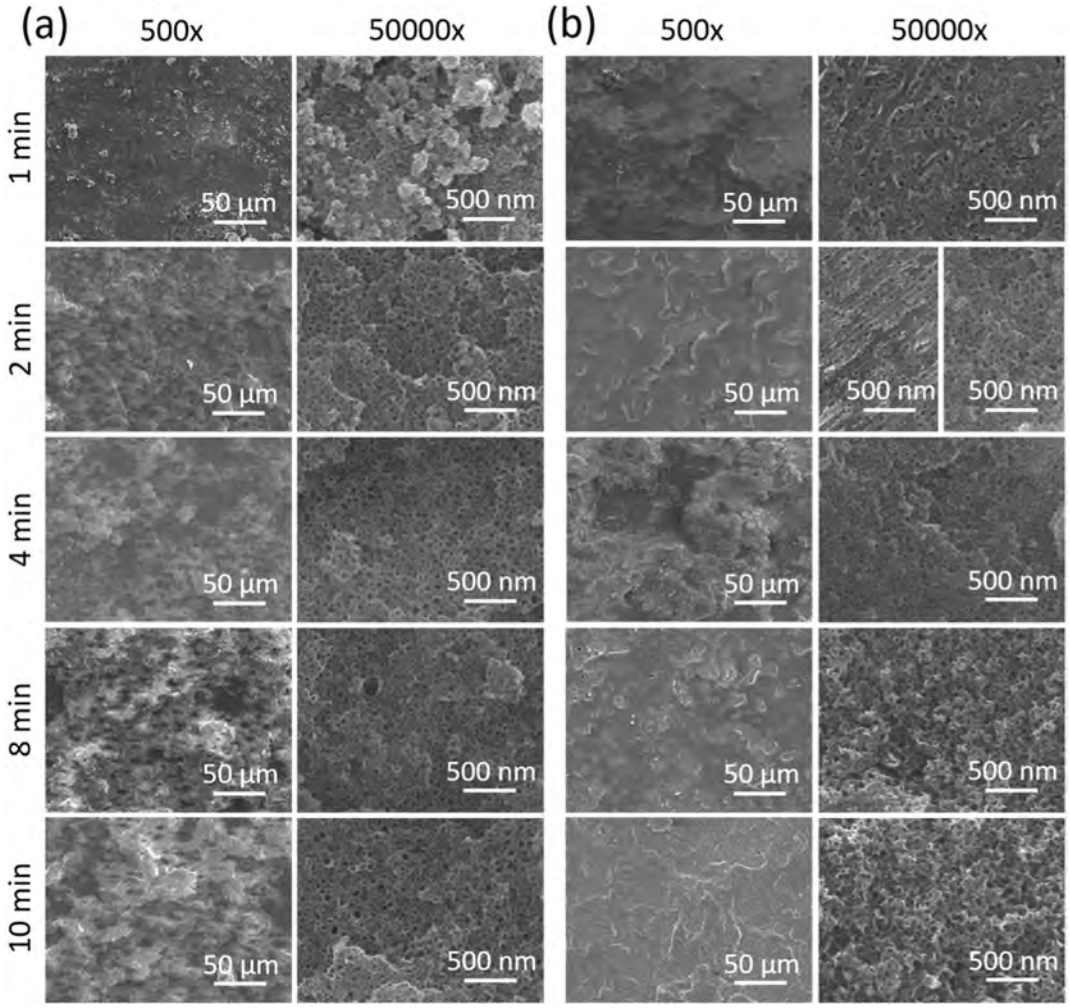

Fig. 3. Surface SEM images of the samples anodized at (a) 40 V and (b) 70 V for different anodization time in the electrolyte composed of glycerol, 10 vol% H_2O, and 0.6 M NaCl. The left high-magnification image of the sample anodized at 70 V for 2 min shows the morphology of the unpeeled region and the right one shows the morphology of the peeled region.

prepared by anodizing NiTi alloy show the opposite trend when the voltage is between 20 and 50 V. A possible explanation is different etching rates of NiO and TiO_2 under attack from Cl^- during anodization. TiO_2 is more stable than NiO because of its lower free energy of formation [22]. Hence, NiO may be etched preferentially in the presence of Cl^-, which is also verified by the EDS results. For example, the atomic ratio of Ni to Ti (Ni/Ti) in the NPs anodized at 30 V is about 0.2, which is far less than the nominal ratio (~1.0) in the NiTi alloy. Increasing the anodization voltage accelerates the dissolution of NiO (for example, the Ni/Ti ratio is about 0.1 when anodized at 50 V), thus thinning the bottom barrier layer and consequently narrowing the pore diameter [17]. However, when the voltage is higher than 50 V, the electrolyte temperatures increase gradually (Fig. 2(f)) as a result of the Joule heating effect (Fig. 2(d)). On the one hand, this may lower the viscosity of the electrolyte, facilitating H_2O transportation to widen the NP diameter. On the other hand, it may also facilitate the preferential etching of NiO with resulting thinning of the bottom barrier layer, leading to a narrowing of the NP diameter. Accordingly, these effects offset each other, suggesting that Joule heating has little influence on the NP diameter.

The growth of an irregular surface layer during the initial stage of anodization is well known and subsequent growth of the ordered structure (NTs or NPs) underneath the layer may be a natural selection process [23]. Several measures can be used to eliminate the irregular surface layer, including extending the anodization time [24], elevating the anodization temperature [21] or ultrasonic vibration. The first of these is ineffective in removing the surface layer for Ni–Ti–O NPs fabricated in the EG-based electrolyte [14] and the other two approaches also do not work well (data not shown). However, the present work demonstrates that the use of a glycerol-based electrolyte can solve the problem. Two possible removal mechanisms based on the variation in the anodization voltage may be proposed. During anodization, the thickness (d) of irregular surface layer is determined by $d = fU$, where f is the growth factor of the oxide and U is the applied voltage [12]. At a low voltage (20–40 V), d is relatively small and under attack by Cl^-; the layer is partially dissolved and/or detached from the substrate by forming nanoparticles (see the high-magnification image of the sample anodized for 1 min in Fig. 3(a)). The smoke-like substance in the beakers could be due to the detached nanoparticles when the samples are anodized at 20–40 V in Fig. 2(c). In contrast, when the voltage is raised to 50–90 V, d is relatively large so that the irregular layer is not so vulnerable to attack by Cl^- (see the high-magnification image of the sample anodized for 1 min in Fig. 3(b)). However, because of the internal stress between the irregular layer and the growing NPs, and interfacial weakening under attack by Cl^- at a high temperature (Fig. 2(f)) induced by current self-amplification (run-away anodization) (Fig. 2(d)) [25], the irregular layer delaminates from the NPs (see low-magnification images of the anodized samples in Fig. 3(b)). Peeling is verified by the presence of a yellow substance in the beakers after anodization at 50–90 V (Fig. 2(c)) and the current oscillations observed during anodization (Fig. 2(d)).

5. Conclusion

Ni–Ti–O NPs with different diameters have been fabricated on NiTi alloy by anodization in a glycerol electrolyte containing 10 vol% H_2O and 0.6 M NaCl. The viscous glycerol offers a buffer system for transportation of Cl^- and H_2O to the electrode/electrolyte interface, providing a larger voltage window (20–80 V) for the fabrication of NPs with a tunable diameter (23–39 nm). At a low voltage, removal of the irregular surface layer may be due to dissolution arising from chemical etching, whereas at a high voltage, it may be a result of peeling due to internal stress.

Acknowledgements

This work was jointly supported by the National Natural Science Foundation of China (31400815, 51671140), Hong Kong Research Grants Council (RGC) General Research Funds (GRF) No. CityU 11301215, City University of Hong Kong Applied Research Grant (ARG) No. 9667122, and City University of Hong Kong Strategic Research Grant (SRG) No. 7004644.

References

[1] J.-H. Kim, K. Zhu, Y. Yan, C.L. Perkins, A.J. Frank, Microstructure and pseudocapacitive properties of electrodes constructed of oriented NiO-TiO_2 nanotube arrays, Nano Lett. 10 (2010) 4099–4104.
[2] Z. Li, D. Ding, Q. Liu, C. Ning, Hydrogen sensing with Ni-doped TiO_2 nanotubes, Sensors-Basel 13 (2013) 8393–8402.
[3] Z. Li, D. Ding, Q. Liu, C. Ning, X. Wang, Ni-doped TiO_2 nanotubes for wide-range hydrogen sensing, Nanoscale Res. Lett. 9 (2014) 118.
[4] R. Hang, Y. Liu, A. Gao, L. Bai, X. Huang, X. Zhang, N. Lin, B. Tang, P.K. Chu, Highly ordered Ni–Ti–O nanotubes for non-enzymatic glucose detection, Mater. Sci. Eng. C 51 (2015) 37–42.
[5] G.-Y. Hou, Y.-Y. Xie, L.-K. Wu, H.-Z. Cao, Y.-P. Tang, G.-Q. Zheng, Electrocatalytic performance of Ni-Ti-O nanotube arrays/NiTi alloy electrode annealed under H_2 atmosphere for electro-oxidation of methanol, Int. J. Hydrog. Energy 41 (2016) 9295–9302.
[6] H. He, G. Ke, P. He, J. Liang, F. Dong, Ordered NiO–TiO_2 nanotube arrays as an efficient catalyst support for methanol oxidation, Phys. Status Solidi A 212 (2015) 2085–2090.
[7] R. Hang, X. Huang, L. Tian, Z. He, B. Tang, Preparation, characterization, corrosion behavior and bioactivity of Ni_2O_3-doped TiO_2 nanotubes on NiTi alloy, Electrochim. Acta 70 (2012) 382–393.
[8] Z. Huan, L. Fratila-Apachitei, I. Apachitei, J. Duszczyk, Synthesis and characterization of hybrid micro/nano-structured NiTi surfaces by a combination of etching and anodizing, Nanotechnology 25 (2014) 055602.
[9] R. Hang, Y. Liu, S. Liu, L. Bai, A. Gao, X. Zhang, X. Huang, B. Tang, P.K. Chu, Size-dependent corrosion behavior and cytocompatibility of Ni–Ti–O nanotubes prepared by anodization of biomedical NiTi alloy, Corros. Sci. 103 (2016) 173–180.
[10] P.P. Lee, A. Cerchiari, T.A. Desai, Nitinol-based nanotubular coatings for the modulation of human vascular cell function, Nano Lett. 14 (2014) 5021–5028.
[11] P.P. Lee, T.A. Desai, Nitinol-based nanotubular arrays with controlled diameters upregulate human vascular cell ECM production, ACS Biomater Sci. Eng. 2 (2016) 409–414.
[12] P. Roy, S. Berger, P. Schmuki, TiO_2 nanotubes: synthesis and applications, Angew. Chem. Int. Ed. 50 (2011) 2904–2939.
[13] R. Hang, Y. Liu, L. Zhao, A. Gao, L. Bai, X. Huang, X. Zhang, B. Tang, P.K. Chu, Fabrication of Ni-Ti-O nanotube arrays by anodization of NiTi alloy and their potential applications, Sci. Rep. 4 (2014) 7547.
[14] R. Hang, M. Zong, L. Bai, A. Gao, Y. Liu, X. Zhang, X. Huang, B. Tang, P.K. Chu, Anodic growth of ultra-long Ni-Ti-O nanopores, Electrochem. Commun. 71 (2016) 28–32.
[15] D. Kim, A. Ghicov, P. Schmuki, TiO_2 nanotube arrays: elimination of disordered top layers ("nanograss") for improved photoconversion efficiency in dye-sensitized solar cells, Electrochem. Commun. 10 (2008) 1835–1838.
[16] J. Park, S. Bauer, K. von der Mark, P. Schmuki, Nanosize and vitality: TiO_2 nanotube diameter directs cell fate, Nano Lett. 7 (2007) 1686–1691.
[17] S. Bauer, S. Kleber, P. Schmuki, TiO_2 nanotubes: tailoring the geometry in H_3PO_4/HF electrolytes, Electrochem. Commun. 8 (2006) 1321–1325.
[18] W. Lee, R. Ji, U. Gösele, K. Nielsch, Fast fabrication of long-range ordered porous alumina membranes by hard anodization, Nat. Mater. 5 (2006) 741–747.
[19] J.M. Macak, P. Schmuki, Anodic growth of self-organized anodic TiO_2 nanotubes in viscous electrolytes, Electrochim. Acta 52 (2006) 1258–1264.
[20] H.E. Prakasam, K. Shankar, M. Paulose, O.K. Varghese, C.A. Grimes, A new benchmark for TiO_2 nanotube array growth by anodization, J. Phys. Chem. C 111 (2007) 7235–7241.
[21] D. Wang, Y. Liu, B. Yu, F. Zhou, W. Liu, TiO_2 nanotubes with tunable morphology, diameter, and length: synthesis and photo-electrical/catalytic performance, Chem. Mater. 21 (2009) 1198–1206.
[22] S.A. Shabalovskaya, G.C. Rondelli, A.L. Undisz, J.W. Anderegg, T.D. Burleigh, M.E. Rettenmayr, The electrochemical characteristics of native Nitinol surfaces, Biomaterials 30 (2009) 3662–3671.
[23] K. Yasuda, J.M. Macak, S. Berger, A. Ghicov, P. Schmuki, Mechanistic aspects of the self-organization process for oxide nanotube formation on valve metals, J. Electrochem. Soc. 154 (2007) C472–C478.
[24] G.A. Crawford, N. Chawla, Porous hierarchical TiO_2 nanostructures: processing and microstructure relationships, Acta Mater. 57 (2009) 854–867.
[25] C.Y. Lee, K. Lee, P. Schmuki, Anodic formation of self-organized cobalt oxide nanoporous layers, Angew. Chem. Int. Ed. 52 (2013) 2077–2081.